

The search for the nuclear symmetry energy in reaction dynamics

Giuseppe Verde

INFN, Sezione di Catania, 64 Via Santa Sofia, I-95123, Catania, Italy
E-mail: verde@ct.infn.it

ABSTRACT

This lecture is devoted to the study of the symmetry energy in nuclear matter by means of heavy-ion collisions (HIC). The symmetry energy plays a key role in both nuclear physics and nuclear astrophysics. At intermediate beam energies, $E/A < 100$ MeV, nuclear systems at densities around and below saturation ($\rho < \rho_0 \approx 0.16 \text{ fm}^{-3}$) are produced. A number of observables exhibit a strong sensitivity to the density dependence of the symmetry energy and will be discussed. In particular results from isoscaling, isospin fractionation, neutron/proton pre-equilibrium emissions and isospin transport will be shown to provide important constraints on the density dependence of the symmetry energy. A brief description of theoretical and analysis tools and experimental setups for symmetry energy research will be provided.

I – INTRODUCTION

The study of nuclear dynamics allows one to investigate on the Equation of State (EoS) of nuclear matter (NM), i.e. the relation between pressure, p , temperature, T , and density, ρ . The EoS is important in nuclear physics because it is directly related to the details of the nuclear interaction, similarly to what happens with ordinary everyday matter where Van der Waals forces produce phase diagrams with liquid-gas phase transitions.

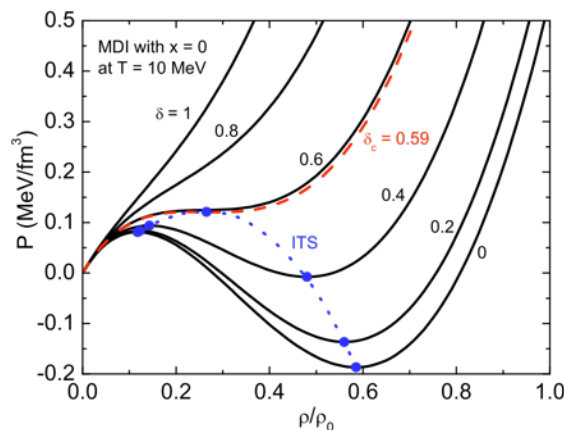


Fig. 1. Isothermal (constant temperature $T=10$ MeV) EoS of nuclear matter. Taken from Ref. [1].

Fig. 1 shows a typical Pressure-Density (P - ρ) phase-diagram of infinite nuclear matter calculated within a specific assumption about the forces acting between nucleons [1]. A fixed temperature of $T=10$ MeV is assumed in the calculation. The different solid lines correspond to different values of the so-called “isospin asymmetry”, defined as the neutron/proton density asymmetry, $\delta = (\rho_n - \rho_p) / (\rho_n + \rho_p)$, with ρ_n and ρ_p being, respectively the neutron and proton densities. $\delta=0$ corresponds to

“symmetric nuclear matter” and NM is unstable in the region where the derivative of the pressure is negative. Similarly to Van der Waals matter, this instability region is characterised by density instabilities and NM stays in a state of liquid-gas coexistence. Studying the EoS of NM allows one to explore the main features of the in-medium nuclear interaction. In this respect an important aspect that one can easily deduce by inspecting Fig. 1 is represented by the fact that the EoS of nuclear matter depends on the isospin asymmetry parameter δ : “asymmetric nuclear matter” ($\delta \neq 0$) behaves very differently as compared to symmetric nuclear matter ($\delta = 0$). This problem is one of the key issues in nowadays nuclear physics research. Indeed, studying the EoS of asymmetric nuclear matter provides tools to explore the poorly known isovector part of the in-medium nuclear interaction accounting for the different behaviour of neutrons and protons.

In the case of infinite nuclear matter one mostly deals with the problem of the role played by the isovector interaction in the nuclear many-body problem. Because of our poor knowledge about the isospin dependence of the in-medium nucleon-nucleon interactions and the difficulties in solving the nuclear many-body problems, predictions on the EOS of isospin asymmetric nuclear matter based on various many-body theories differ widely at both low and high densities [2,3]. Knowledge on the EoS of asymmetric NM is essential for understanding not only many problems in nuclear physics but also a number of important issues in astrophysics such as the nucleosynthesis during pre-supernova evolution of massive stars and the cooling of proton-neutron stars [4]. In this context heavy-ion collisions represent the only terrestrial means to explore the EoS of NM. As it will be explained in the following sections of this lecture, during collisions nuclear matter at both low and high densities is produced and can therefore be explored under laboratory controlled conditions.

In the last decades these studies have been extensively conducted with experiments at different laboratories all over the world. But most of these studies have focused on the properties of nuclear matter with little attention to the isospin degree of freedom, i.e. the asymmetry in neutron-proton density δ (see Fig. 1). The recent availability of beams and target combinations with different N/Z asymmetries have then stimulated the efforts of understanding what happens when compressing and heating asymmetric nuclear matter with $\delta \neq 0$. New phenomena have been discovered and it became clear that little is presently known about the equation of state of asymmetric nuclear matter. The main unresolved issue in this field is represented by the density dependence of the symmetry energy, $E_{\text{sym}}(\rho)$. The symmetry energy and its density dependence, playing a key role in important aspects of nuclear dynamics, is directly linked to the isovector part of the in-medium nuclear interaction and it determines important properties of neutron stars. This wide range of implications have attracted the interest of a large community of nuclear physicists (working in both dynamics and structure) and astrophysicists (See Ref. [5] for a recent review article).

In this lecture an overview of the main attempts to study the symmetry energy and the equation of state of asymmetric nuclear matter will be presented. The main focus will be devoted to the symmetry energy at sub-saturation densities, $\rho < \rho_0$, accessible in heavy-ion collisions at intermediate energies ($E/A < 100$ MeV). At these energies and densities an extensive amount of investigations have been conducted and make it possible to draw some conclusions about the present status and the work we need to do in the coming future with the availability of radioactive ion beam facilities. It must be also mentioned that the symmetry energy at super-saturation density, $\rho > \rho_0$, is still largely unconstrained. This matter will be the subject of extensive experimental campaigns at the FAIR (Germany) and RIKEN (Japan) facilities in the future and the existing experimental signatures are still difficult to interpret in order to draw definitive conclusions.

Because of limited space in this lecture we will not cover this topic of high density NM, even if the reader is invited to read the literature and explore the main issues related to research performed with heavy-ion collisions at incident energies $E/A > 200$ MeV. The next section will introduce the definition of the symmetry energy and the tools required to study its density dependence in nuclear dynamics. The following sections will present the results obtained with different experimental probes. Finally a status of our present knowledge about the symmetry energy will be discussed, with a “look forward” to future investigations at higher energies and with radioactive beams.

II – WHAT IS THE SYMMETRY ENERGY?

The EoS of asymmetric nuclear matter at zero-temperature is the relation between energy, density and isospin asymmetry at $T=0$. This relation can be parameterized with the following expression:

$$E(\rho, \delta) = E(\rho, \delta = 0) + E_{sym}(\rho) \cdot \delta^2 \quad (1)$$

In this expression, E is the energy, $\rho = \rho_n + \rho_p$ is the total density (with ρ_n and ρ_p being, respectively, the neutron and proton densities) and $\delta = (\rho_n - \rho_p) / (\rho_n + \rho_p)$ is the isospin asymmetry. $\delta = 0$ represents symmetric nuclear matter ($\rho_n = \rho_p$). Neutron-rich and proton-rich matter will be characterised, respectively, by $\delta > 0$ and $\delta < 0$. Eq. (1) consists of an expansion to second order of the energy around $\delta = 0$ (i.e. around symmetric nuclear matter) and states that the EoS for asymmetric nuclear matter is composed by the sum of the EoS for symmetric nuclear matter, $E(\rho, \delta = 0)$, and the “asymmetry term”, $E_{sym}(\rho) \cdot \delta^2$. Due to this last term, the EoS of NM depends on isospin asymmetry, δ . The function $E_{sym}(\rho)$ is called “symmetry energy” and depends on the “isoscalar density”, $\rho = \rho_n + \rho_p$. It is easily deduced from Eq. (1) that the effects of the symmetry energy become important for isospin asymmetric nuclear matter, i.e. for large values of isospin asymmetry, δ . Indeed the asymmetry term of the EoS in Eq. (1) increases as the square of δ .

Most of the investigations carried out so far have been focusing on the study of the EoS for symmetric nuclear matter, $\delta = 0$, leaving the density dependence of the symmetry energy largely unconstrained. However, the symmetry energy is one of the most important quantities in nuclear physics. A symmetry energy term is already known in undergraduate nuclear physics courses when the Bethe-Weiszacker (BW) formula of nuclear binding energies is studied [6]. The binding energy of a nucleus of mass number A , charge Z and neutron number N ($A = Z + N$), contains

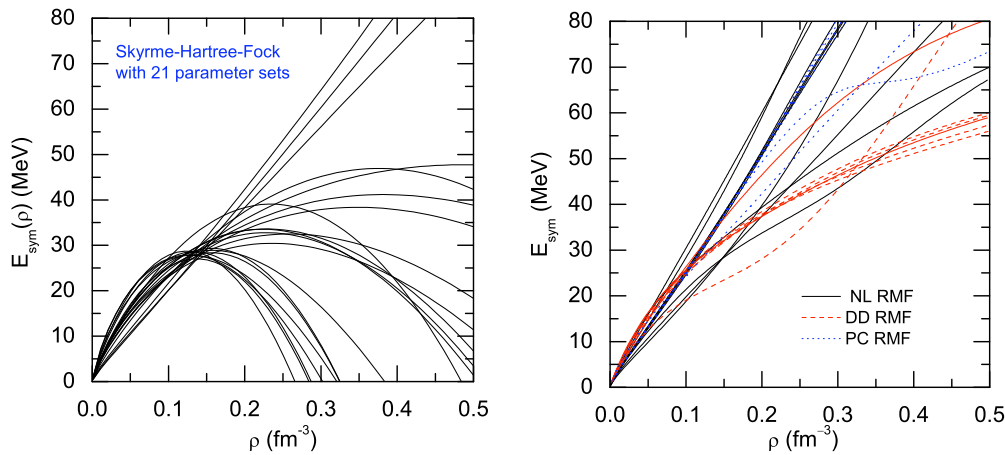


Fig. 2. Left window: density dependence of the nuclear symmetry energy $E_{sym}(\rho)$ from Skyrme-Hartree-Fock (SHF) calculations using different forms of Skyrme interactions. Right window: Same as in left panel when using different types of relativistic mean field (RMF) models. Taken from [5].

different contributions provided by its volume, surface, Coulomb repulsion between the constituent nucleons and, finally, on the symmetry energy component, E_{sym}/A . This symmetry energy component is given by $C_{sym} \cdot [(N-Z)/(N+Z)]^2$. This last expression resembles the symmetry term, $E_{sym}(\rho) \cdot \delta^2$, in Eq. (1) very closely. Indeed, in a finite nucleus at normal saturation density the isospin asymmetry, δ , can be associated to the N/Z asymmetry of the nucleus, $\delta = (N-Z)/(N+Z)$. The value of C_{sym} in the BW formula is about 30 MeV. It corresponds to the value of the symmetry energy $E_{sym}(\rho_0)$ at saturation density, $\rho = \rho_0$. So far we only roughly know the value of the symmetry energy at saturation, $C_{sym} = E_{sym}(\rho_0) \approx 30$ MeV. The symmetry energy at sub-saturation ($\rho < \rho_0$) and super-saturation ($\rho > \rho_0$) densities is still largely unconstrained.

Fig. 2 shows the results of many different approaches used to calculate the density dependence of the symmetry energy [5]. Due to our poor knowledge of the isovector part of the in-medium nuclear interaction and to difficulties in solving the nuclear many-body problem, different approaches provide completely different results. These uncertainties are directly reflected in unknown important properties of nuclei far from the valley of stability and in uncertainties in the knowledge of certain features of neutron stars. It is customary to expand to second order the symmetry energy into a Taylor series around saturation density:

$$E_{sym}(\rho) = E_{sym}(\rho_0) + \frac{L}{3} \left(\frac{\rho - \rho_0}{\rho_0} \right) + \frac{K_{sym}}{18} \left(\frac{\rho - \rho_0}{\rho_0} \right)^2 \quad (2)$$

where L and K_{sym} are the slope and curvature parameters of the nuclear symmetry energy at $\rho = \rho_0$, i.e.,

$$L = 3\rho_0 \left. \frac{\partial E_{sym}(\rho)}{\partial \rho} \right|_{\rho=\rho_0} \quad \text{and} \quad K_{sym} = 9\rho_0^2 \left. \frac{\partial^2 E_{sym}(\rho)}{\partial^2 \rho} \right|_{\rho=\rho_0} \quad (3)$$

The L and K_{sym} also characterize the density dependence of the symmetry energy, i.e. the shape of the $E_{sym}(\rho)$ around saturation. The expansion reported in Eqs. (2) and (3) allows one to use a

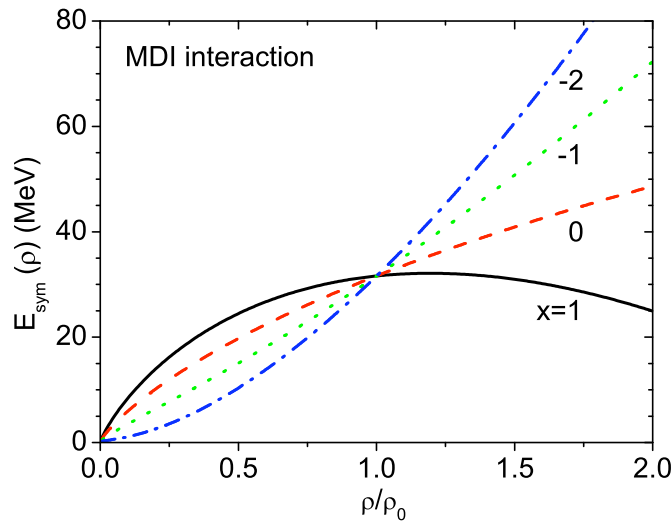


Fig. 3. Density dependence of the symmetry energy in a momentum dependent interaction model [5]

language common to different communities. Indeed the slope parameter L has been found to be correlated linearly with the neutron-skin thickness of heavy nuclei [8-11]. The curvature parameter K_{sym} is strongly related to the incompressibility of asymmetric nuclear matter and its isospin dependence which can be studied asy by measuring the giant monopole resonance (GMR) of neutron-rich nuclei [12-14]. These parameters, especially the L slope, are also of fundamental importance in understanding properties of neutron stars [4,8,11].

In this lecture we will focus on the most powerful investigations on the density dependence of the symmetry energy, i.e. heavy-ion collisions (HIC). During the collision between two heavy-ions one can indeed produce gradients of density, temperature and isospin asymmetry and study their properties under laboratory controlled conditions. In accelerator laboratories one can work with finite nuclei and one can produce portions of nuclear matter with different isospin asymmetries by choosing properly projectile and target nuclei having different neutron/proton N/Z asymmetries. Indeed, Eq. (1) shows that the effects of the symmetry energy are small, as compared to those induced by the symmetric part ($\delta=0$) of the equation of state. It is therefore important to compare observables measured in reactions with different N/Z values in order to better isolate the effects induced by the symmetry energy. These studies also require the use of detectors characterized by high resolution, especially from the point of view of isotopic identification capabilities. These detectors also need to detect all fragments produced during a collision thus implying large solid angle coverage. Eq. (1) states that the effects induced by the isospin-dependent term increase as the square of isospin asymmetry, δ . This is the reason why considerable efforts have been recently invested in studying collisions between nuclei with larger N/Z -asymmetries ($N/Z=1.2-1.5$). These studies have revealed new phenomena that are induced solely by the presence of the asymmetry term of the EoS. The strategy commonly used to investigate the symmetry energy with HIC consists of comparing measured observables to the same quantities calculated by means of specific transport model simulations [5]. In these transport theories it is possible to provide the density dependence of the symmetry energy as an input. Hence comparisons to experimental data

probe different parameterizations of $E_{sym}(\rho)$. Fig. 3 shows a few of these parameterizations that are commonly distinguished as “asy-soft” (such as the solid line labelled $x=1$) and “asy-stiff” (such as

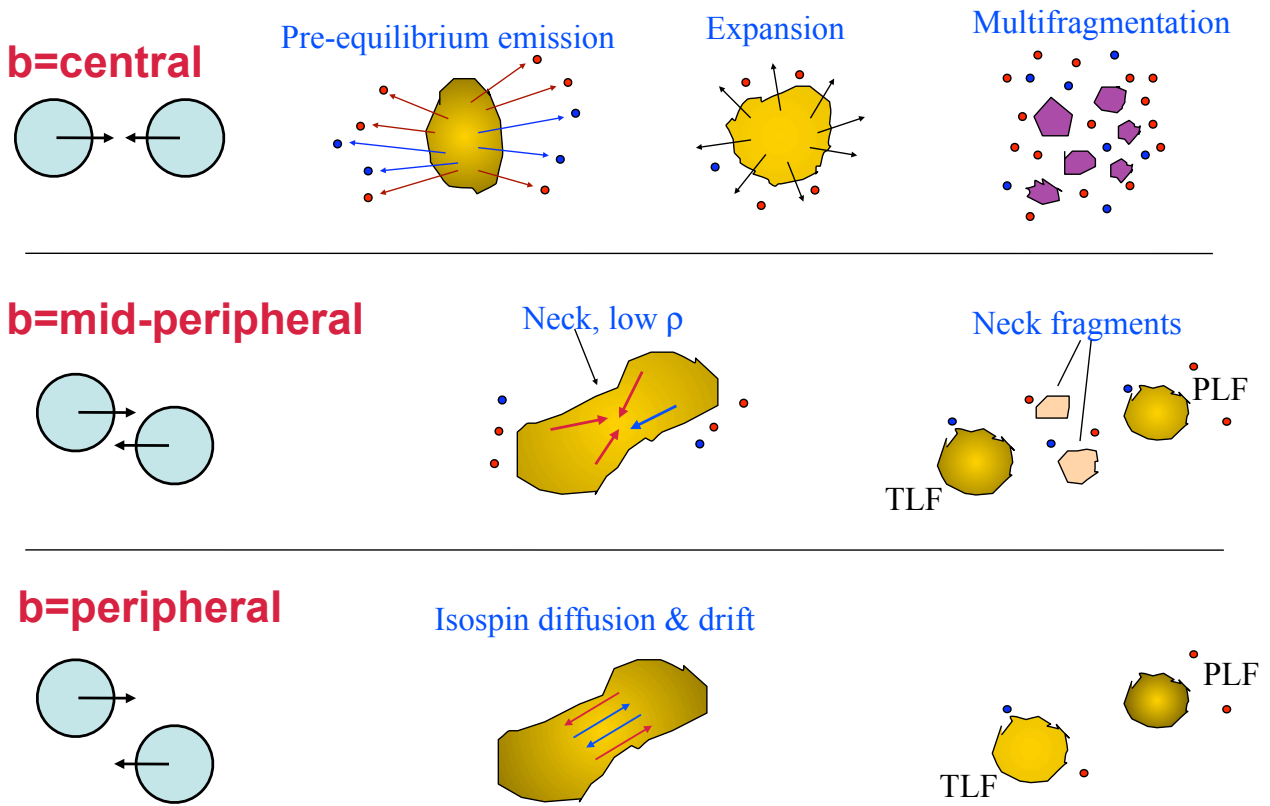


Fig. 4. Schematic drawing of the dynamical evolution of a collision between two heavy ions at intermediate energies and at central (top), mid-peripheral (mid) and peripheral (bottom) impact parameters.

the dot-dashed and dotted lines labelled as $x=-2$ and -1). In dynamical models an extensively used parameterization of the symmetry energy is provided by the equation:

$$E_{sym}(\rho) = C_{sym} \cdot \left(\frac{\rho}{\rho_0} \right)^\gamma \quad (4)$$

with the constant $C_{sym}=25\text{-}30$ MeV corresponding to the value of the symmetry energy at saturation density used in the Bethe-Weiszacker formula. A larger (smaller) value of the constant γ corresponds to a stiff (soft) density dependence of the symmetry energy. Therefore the problem of determining the density dependence of the symmetry energy is simplified, within the context of these dynamical models, with that of determining the γ parameter with comparisons of model simulations to experimental data. Even if this is a considerable (and probably too strong) simplification it still provides most of the interesting physics content in isospin dependent nuclear dynamics. The x -parameter label reported close to the curves on Fig. 3 contains information about the degree of stiffness of the density dependence of the symmetry energy

III – HEAVY-ION COLLISIONS AND THE SYMMETRY ENERGY

Heavy-ion collisions have been extensively studied over the last decades. Fig. 4 shows a schematic drawing of phenomena occurring during the dynamical evolution of a collision between two nuclei at energies $E_{beam}<100$ MeV/nucleon and at different impact parameters, b . At fixed beam energies, one observes very different phenomena at different impact parameters. The

literature in this field is very wide and beyond the scope of this lecture. However it is important to lay down a few key issues regarding the determination of the impact parameter. Indeed we do not have a direct access to the impact parameter. We only measure the energy and angle distribution of fragments and light particles produced in each collisions event as Fig. 4 schematically shows. Therefore experimentally one can only measure observables that are reasonably connected to the impact parameter because they probe the violence of the collision. More violent interactions between projectile and target occur in head-on collisions ($b=0$, upper panel on Fig. 4) while more gentle interactions are typically explored at mid-central and peripheral collisions ($b>0$, depending on the specific reaction to be studied, middle and bottom panels on Fig. 4). Plenty of observables have been used to probe the violence of the collision and extract information about the impact parameter [16,17]. Among them we mention the multiplicity of charged particles, N_C , and the total

transverse kinetic energy, $E_T = \sum_{i=1}^{N_C} E_i \sin^2 \theta_i$, with E_i and θ_i being, respectively, the kinetic energy

and polar angle of particle i produced in the event. These observables measure the violence of the collision event. More violent collisions produce a larger amount of charged particles (larger N_C) and more particles are emitted in the transverse direction (larger E_T), corresponding to smaller impact parameters b . In contrast, collisions at large b produce less particles in the final state (small N_C) and the events result more elongated in beam direction with correspondingly small transverse energies (small E_T). The choice of N_C or E_T mostly depend on the specific reaction to be studied and on the features of the used experimental setup. Modern 4π detectors, such as INDRA [18] or CHIMERA [19] have introduced more complete and reliable impact parameter filters thanks to their high solid angle coverage and high quality performances [20,21]. A useful quantity that will be extensively used in this lecture is represented by the so-called “reduced impact parameter”,

$\hat{b} = b / b_{\max}$, where $b_{\max} = R_{\text{proj}} + R_{\text{targ}}$, with R_{proj} and R_{targ} being the radii of the projectile and target

nucleus, respectively. This reduced impact parameter definition is suggested by simple geometric consideration about the collision between two nuclei and it can be considered as a useful quantity at intermediate energies. Most of the results presented in this lecture have been collected in

“central collisions”, typically defined as collisions at reduced impact parameters of $\hat{b} < 0.3$ (top

panel on Fig. 4), or “peripheral collisions”, typically defined by reduced impact parameters $\hat{b} > 0.7$

(bottom panel on Fig. 4). In between these two limits a very interesting impact parameter range

exists, commonly referred to as “mid-peripheral”, and roughly associated to $0.4 < \hat{b} < 0.7$ (middle panel on Fig. 4). These limits are here only schematically presented and they change depending on the specific experiment that one is conducting.

In the case of central collisions (top part of Fig. 4), nuclear matter is first compressed to densities higher than the saturation value, $\rho_0 = 0.16 \text{ fm}^{-3}$, and heated to temperatures as high as $T \approx 10 \text{ MeV}$, both these limits depending on the incident energy. Due to the repulsive core of the nuclear force, the early compression stage is followed by an expansion phase toward lower densities (as low as $\rho < 0.1 \cdot \rho_0 \text{ fm}^{-3}$) and nuclear matter cools down. During this process a significant number of neutrons, protons and light particles can be emitted as a consequence of a large number of dynamical nucleon-nucleon collisions. These particles are commonly called “pre-equilibrium emissions”. When nuclear matter reaches low densities after the expansion phase, it may enter instability regions where it undergoes the so-called “multifragmentation” phenomenon.

Multifragmentation has been often associated to an experimental signature of a liquid-gas phase transition in nuclear matter [15]. In this “phase-transition view of multifragmentation, the “liquid” phase would be represented by nuclei in their ground state and at saturation density while the “gas” phase is associated to systems of free nucleons and light particles produced in energetic collisions where nuclear matter is entirely broken up into pieces (vaporization). At the very final stages of the collision process fragments produced during multifragmentation phenomena may still be excited to internal unbound states. In this case they may undergo the so-called “secondary decay” phenomena producing a delayed emission of light particles.

In peripheral collisions (bottom panel on Fig. 4) the reaction mostly maintain a binary character with the exception of light particle and free nucleons emitted as pre-equilibrium particles [22]. The two main fragments in the final state are residues of the initial projectile and target nuclei, and they are commonly referred to as quasi-projectile (QP) and quasi-target (QT) or projectile-like fragment

(PLF) and target-like fragment (TLF), respectively. During the time of interaction between projectile and target a massive transfer of nucleons and energy can occur leading to excited QP and QT fragments that can further decay by light particle emission or even by undergoing multifragmentation if the excitation energy is high enough. The exchange of nucleons between QP and QT is also responsible for a modification of the neutron/proton N/Z balance of the initial interacting nuclei. As we will see on Section IV, this exchange of neutrons and protons can lead to isospin equilibration or transparency as a consequence of the effects induced by the density dependence of the symmetry energy.

In mid-peripheral collisions (middle panel on Fig. 4) a spectacular phenomenon has been observed experimentally, consisting of the emission of fragments from the neck connecting the two projectile and target nuclei. This phenomenon has been termed “neck emission” and is repository of very interesting physics phenomena related to the symmetry energy [23-27].

The next Section will focus on probes of the symmetry energy in central collisions while peripheral and mid-peripheral collisions will be the subject of Section IV.

III – ISOSPIN EFFECTS AND THE DENSITY DEPENDENCE OF THE SYMMETRY ENERGY IN CENTRAL COLLISIONS

Central collisions between heavy ions have been extensively studied. Regardless the very rich amount of physics that we have learnt from these systems, in this lecture we will focus on the following phenomena that are connected to the symmetry energy of nuclear matter: A) Isoscaling and isospin fractionation; B) Neutron-proton pre-equilibrium emission. Isoscaling and isospin fractionation (Section III.A) are related to the late multifragmentation stage of the collision (right side of top panel on Fig. 3) and to the occurrence of a liquid-gas phase transition in nuclear matter. In contrast, pre-equilibrium emission (Section III.B) occurs in the early stage of the reaction (left side of top panel on Fig. 3) and has been probably provided among the strongest probes of the symmetry energy and its density dependence.

III.A Isoscaling and isospin fractionation

As already mention in the previous section heavy-ion collisions may lead to the production of a significant number of intermediate mass fragments that have been often regarded as an evidence of liquid-gas coexistence in nuclear matter. Early studies on multifragmentation did not pay too much attention to the problem of their isospin content but rather focused on their absolute yields and elemental distributions. The recent investigations of the properties of asymmetric nuclear

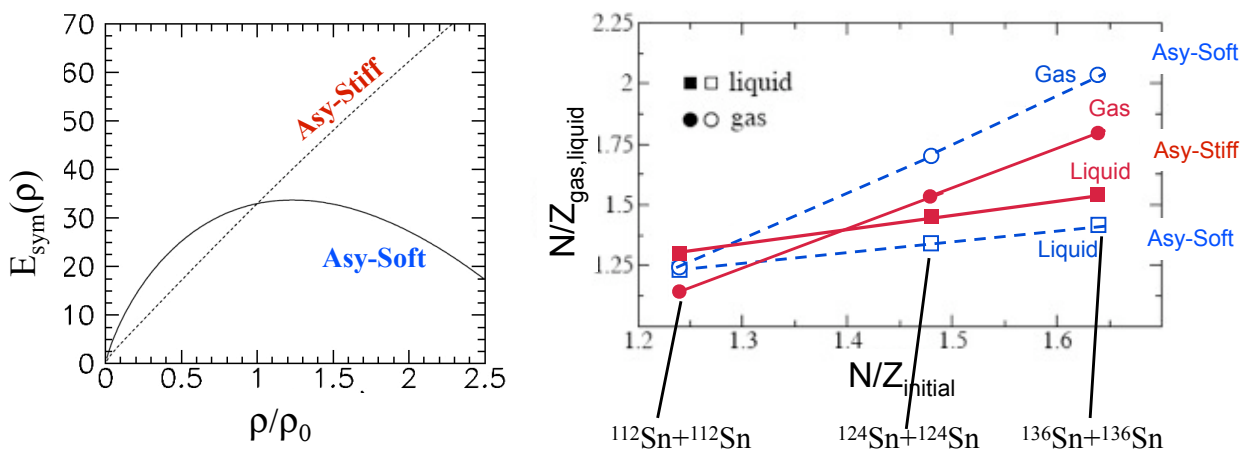


Fig. 5. Left window: typical asy-stiff and asy-soft density dependence of the symmetry energy. Right window: isospin fractionation in a dynamical model of heavy-ion collisions (see text for details).

matter has in contrast shown that the isospin degree of freedom plays a key role. In particular it was shown that in neutron-rich matter one expects to observe a non-equal partition of the system's

isospin asymmetry with the gas phase being more neutron-rich than the liquid phase [28]. This phenomenon is commonly referred to as “isospin fractionation” or “isospin distillation”. Regardless early indications of isospin fractionation existed, only recently progress has been made with experiments performed at the NSCL of Michigan State University (USA), the Cyclotron Laboratory of the Texas A&M University (USA), the GSI laboratory of Darmstadt (Germany), GANIL (France) and the INFN-LNS of Catania (Italy). Fig. 5 (left side) shows two simplified parameterizations of the symmetry energy (Asy-Stiff and Asy-Soft) often used in SMF (Stochastic Mean Field) dynamical model calculations by V. Baran, M. Colonna et al. [29]. These different density dependence of E_{sym} were plugged in as input to simulations of central $^{112}\text{Sn}+^{112}\text{Sn}$, $^{124}\text{Sn}+^{124}\text{Sn}$ and $^{136}\text{Sn}+^{136}\text{Sn}$ collisions at $E/A=50$ MeV and the results are shown on the right panel of Fig. 5. These three reaction systems were chosen because they all contain the same amount of protons ($Z_{\text{initial}}=Z_{\text{projectile}}+Z_{\text{target}}=100$) but differ by their number of neutrons and, therefore, by the N/Z -asymmetry ($N/Z_{\text{initial}}=1.24, 1.36$ and 1.48 for $^{112}\text{Sn}+^{112}\text{Sn}$, $^{124}\text{Sn}+^{124}\text{Sn}$ and $^{136}\text{Sn}+^{136}\text{Sn}$ systems, respectively). Differences observed when moving from one reaction system to the other should allow one to better emphasize effects induced solely by the density dependence of the symmetry energy [according to what is expected by the δ^2 dependence of Eq. (1)]. The SMF model simulation shows that the collision and the initial compression are followed by an expansion of the composite nuclear source. Along this expansion, small density fluctuations are amplified by the unstable mean-field and large amplitude density gradients are developed. This process ends up with the formation of several fragments, corresponding to the high density bumps. Several nucleons are emitted, prior to fragmentation, at the early stage (pre-equilibrium emission) and/or are evaporated while fragments are formed. Primary fragments are identified in SMF by applying a coalescence procedure to the matter with density larger than $\rho_{\text{cut}}=1/5\rho_0$ (that we classify as ‘liquid phase’). The remaining nucleons are considered as belonging to the ‘gas phase’. The average N/Z of emitted nucleons (gas phase) and of the IMF’s is presented in Fig. 5 (Right Panel) as a function of the initial asymmetry, $(N/Z)_{\text{initial}}$, of the three colliding Sn systems. Generally, the gas phase is seen to be more neutron-rich while the IMF’s are more symmetric. This is due to the combined action of the pre-equilibrium emission, that reduces the neutron excess of the composite system, and of the above mentioned “isospin distillation” or “isospin fractionation” mechanism acting at a later stage, while fragments are formed. This trend is stronger in the Asy-soft relative to the Asy-stiff case. This can be understood by inspecting the left panel of Fig. 5 showing that the symmetry energy is larger below saturation in the Asy-Soft than in the Asy-Stiff case. This effect, caused by the decrease in the symmetry energy when the density gets lower, can be used to investigate the behavior of the derivative of the symmetry energy with respect to density. The difference between the asymmetries of the gas and liquid phases increases with the $(N/Z)_{\text{initial}}$ of the system, and is always larger in the Asy-soft case. It should be noticed that the isotopic content of the gas phase appears more sensitive to the Iso-EoS than the asymmetry of the fragments. As one can see from Fig. 5 (right panel), for the IMF’s the difference between the two EoS’s is just about 8%.

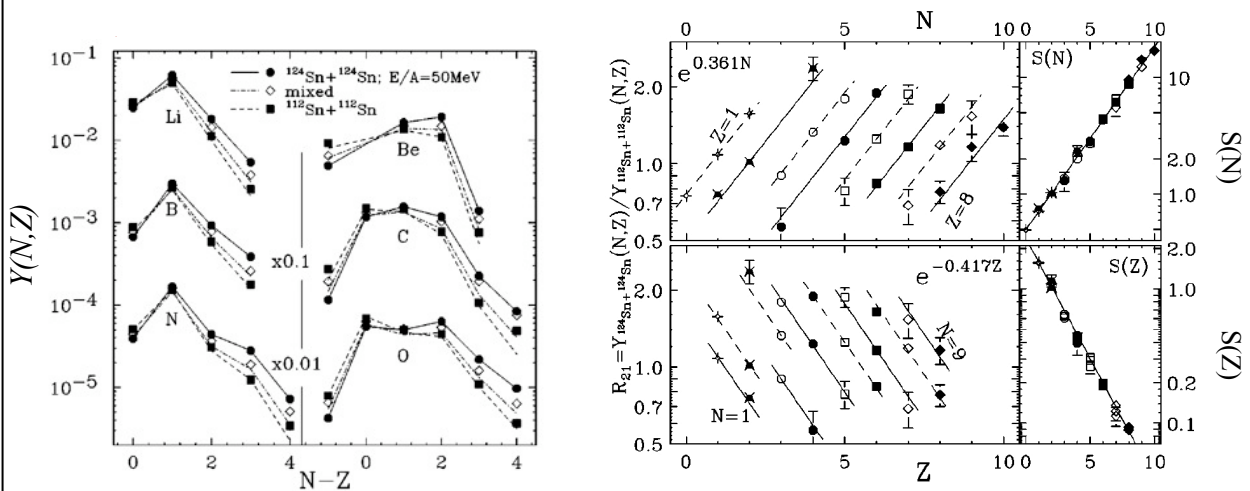


Fig. 6. Left window: isotopic distributions measured in $^{112}\text{Sn}+^{112}\text{Sn}$, $^{112}\text{Sn}+^{124}\text{Sn}$, $^{124}\text{Sn}+^{112}\text{Sn}$ and $^{124}\text{Sn}+^{124}\text{Sn}$ at $E/A=50$ MeV. Right panel: isoscaling plots (see text).

It is important to also mention that isospin distillation is observed in statistical models of multifragmentation as well. For a review see Ref. [30]. However, dynamical models offer the opportunity of using explicit density dependence functional of the symmetry energy at the input stage and are therefore more useful from a didactical point of view.

Dynamical model results obtained with simulations of a realistic reaction system show the dynamical nature of isospin fractionation phenomena predicted to occur in asymmetric nuclear matter, thus supporting the idea of observing similar phenomena experimentally. One of those experiments has been performed at the National Superconducting Cyclotron Laboratory (NSCL) of Michigan State University (MSU) using the LASSA (Large-Area Silicon Strips and CsI(Tl) detector Array) [31] coupled to the Miniball 4π array [32]. The studied reaction systems were $^{112}\text{Sn}+^{112}\text{Sn}$, $^{112}\text{Sn}+^{124}\text{Sn}$, $^{124}\text{Sn}+^{112}\text{Sn}$ and $^{124}\text{Sn}+^{124}\text{Sn}$ at $E/A=50$ MeV, with an N/Z_{total} ranging between 1.24 and 1.48. Fragments produced in the studied reactions are isotopically resolved (i.e. both their mass number A and charge number Z are measured) and isotopic distributions are constructed. The different data symbols on the left panel of Fig. 6 refer to different reaction systems. The isotopic distributions, $Y(N,Z)$, are represented as a function of the neutron/proton number difference, $N-Z$, for each element $Z=3, 4, 5, 6, 7$ and 8 . It is shown that more neutron rich fragments are produced when more neutron-rich reaction systems are studied. This is quite expected. However, this apparently trivial behavior is enriched by observing a very interesting “scaling law” when the isotopic distributions measured in each reaction system are normalized to those measured in reference reaction such as the most neutron poor $^{112}\text{Sn}+^{112}\text{Sn}$ system. In particular the right panel of Fig. 6 shows the ratios

$$R_{21} = \frac{Y_{^{124}\text{Sn}+^{124}\text{Sn}}(N,Z)}{Y_{^{112}\text{Sn}+^{112}\text{Sn}}(N,Z)} \quad (5)$$

obtained with the yields measured in the $^{124}\text{Sn}+^{124}\text{Sn}$ and $^{112}\text{Sn}+^{112}\text{Sn}$ reaction systems. The top panel shows the ratios R_{21} as a function of neutron number N for each element Z (relative isotopic distributions), while the bottom panel shows the same ratios as a function of the proton number Z for fixed neutron numbers N (relative isotonic distributions). The different isotopes (isotones) lay along parallel lines all at the same distance from one another. This spectacular scaling law has been termed “isoscaling” [33] and suggests that all isotopic and isotonic distributions can be

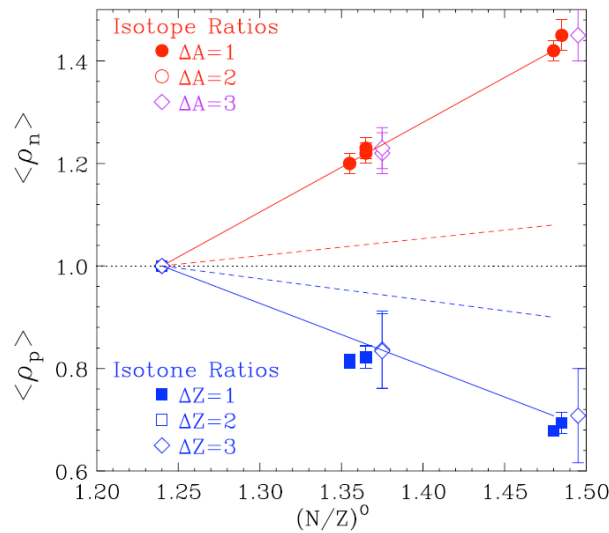


Fig. 7. Normalized free neutron (top) and free proton (bottom) densities in the $^{112,124}\text{Sn}+^{112,124}\text{Sn}$ collisions at $E/A=50$ MeV

described by a universal simple scaling law

$$R_{21} = \frac{Y_{^{124}\text{Sn}+^{124}\text{Sn}}(N,Z)}{Y_{^{112}\text{Sn}+^{112}\text{Sn}}(N,Z)} = C \cdot \exp(\alpha N + \beta Z) \quad (6)$$

depending only on three parameters: a normalization constant, C , and two numbers, α and β , corresponding to the slopes of, respectively, the Z and N relative distributions shown on the top and bottom panels of the right window of Fig. 6. Isoscaling has proved to be very robust and has been observed in many different types of reactions, such as multifragmentation, light ion-induced fragmentation, evaporation and deep-inelastic reactions [33-35]. There are also reports on the observation of isoscaling in spallation reactions [41] and in fission [42].

Eq. (6) can be further simplified by using the "isoscaling function" $S(N)=R_{21} \cdot \exp(-\beta Z)$ that removes the Z dependence and allows one to plot all the experimental isotopic distributions in a more compact way as it is shown on the rightmost top panel of Fig. 6. Similarly one can compact Eq. (6) by multiplying R_{21} by $\exp(-\alpha Z)$ and the resulting experimental data can be represented as a function of Z only (bottom right panel on the right window on Fig. 6).

The most important aspect of isoscaling is its connection to the symmetry energy and the temperature of the system. Isoscaling arises very naturally within a statistical grand-canonical description of fragment production [38]. In particular it can be shown that the isoscaling ratio R_{21} can be expressed as

$$R_{21}(N, Z) = (\hat{\rho}_n)^N (\hat{\rho}_p)^Z \quad (7)$$

where $\hat{\rho}_n = \rho_{free,n}^{124Sn+124Sn} / \rho_{free,n}^{112Sn+112Sn}$ and $\hat{\rho}_p = \rho_{free,p}^{124Sn+124Sn} / \rho_{free,p}^{112Sn+112Sn}$ are the relative free neutron and free proton densities, respectively. In other words $\hat{\rho}_n$ represents the ratio between the density of neutrons in the gas phase in the neutron rich reaction system ($^{124}Sn+^{124}Sn$) and the neutron poor reaction system ($^{112}Sn+^{112}Sn$). Similarly $\hat{\rho}_p$ represents the ratio between the density of

protons in the gas phase in the neutron rich reaction system ($^{124}Sn+^{124}Sn$) and the neutron poor reaction system ($^{112}Sn+^{112}Sn$). By comparing Eq. (6) and (7) it follows that fitting the experimental R_{21} ratios one can use the obtained free parameters α and β to directly extract the normalized free neutron and free proton densities, $\hat{\rho}_n$ and $\hat{\rho}_p$, in the studied reactions. These are represented on

Fig. 7 (data symbols) [38] as a function of the N/Z of the total reaction systems, $(N/Z)_0=1.24, 1.36$ and 1.48 , respectively for $^{112}Sn+^{124}Sn$, $^{112}Sn+^{124}Sn$ and $^{124}Sn+^{124}Sn$ [38]. $\hat{\rho}_n$ ($\hat{\rho}_p$) is observed to

increase (decrease) with increasing $(N/Z)_0$. If the total amount of neutrons and protons in the initial system were distributed uniformly at fragmentation stage among the fragments (liquid-phase) and the free nucleons (gas-phase), the relative neutrons and protons would follow the dashed lines on Fig. 7. Therefore, the reaction behaves in such a way that the neutron/proton asymmetry of the gas phase (data symbols) is larger than initial asymmetry of the system: the liquid-phase results more symmetric and the gas-phase results more neutron-rich than the total system reaction system. This corresponds to an experimental evidence of isospin fractionation phenomena in asymmetric nuclear matter [38]. As already outline with Fig. 5 this observation is due to an effect of the symmetry energy in the low density region where fragments are formed and the liquid-gas phase coexistence occurs.

Especially the α -slope parameter has received extensive attention by the community because of its links to the density dependence of the symmetry energy and to the temperature of the system. This has been studied with both statistical [39] and dynamical [40] approaches. Within a statistical description of multifragmentation where fragments are formed in a system a chemical and thermal equilibrium at temperature T , the slope parameters are given by $\alpha=\Delta\mu_n/T$ and $\beta=\Delta\mu_p/T$ where $\Delta\mu_n=[\mu_n,^{124}Sn+^{124}Sn - \mu_n,^{112}Sn+^{112}Sn]$ and $\Delta\mu_p=[\mu_p,^{124}Sn+^{124}Sn - \mu_p,^{112}Sn+^{112}Sn]$ are the differences between neutron and proton chemical potentials in the neutron rich and neutron poor reaction system [30,38]. Within this statistical approach it is clear that the α slope parameter is expected to decrease with increasing temperature. Such studies have been performed at Texas A&M University [39] and within statistical and dynamical models [40,41]. Indications from experimental data have shown such dependence of the slope parameters on temperature [39,40,42] and the reported results have actually been used to rather probe the density dependence of the symmetry energy. In Ref. [39] the isoscaling parameter α has been related to the symmetry energy, E_{sym} , through the relation

$$\alpha = \frac{4E_{sym}}{T} \cdot \left(\frac{Z_1^2}{A_1^2} - \frac{Z_2^2}{A_2^2} \right) \quad (8)$$

where, Z_1/A_1 and Z_2/A_2 are the charge and the mass numbers from the two systems used in the numerator and denominator of Eq. (6) and T is the temperature. This relation provides a simple and straightforward connection between the symmetry energy and the fragment isotopic yield distribution. The above equation derived from the statistical and the dynamical models of multifragmentation appears similar in form. But the physical meaning of the terms involved in this equation differ for each model. More details and comments about this link between the slope parameter and the symmetry energy can be found in Refs. [39-41,43]. The problem of extracting the density dependence of the symmetry energy from isoscaling slopes and isospin distillation is indeed very difficult. In statistical models, the Z/A in Eq. (8) corresponds to the charge-to-mass ratio of the initial equilibrated fragmenting system, before it actually breaks up into fragments. Whereas, in dynamical models, it corresponds to the charge-to-mass ratio of the liquid phase at a certain time (≈ 300 fm/c) during the dynamical evolution of the colliding systems. Furthermore, the interpretation of the symmetry energy E_{sym} , in dynamical and statistical models also differs

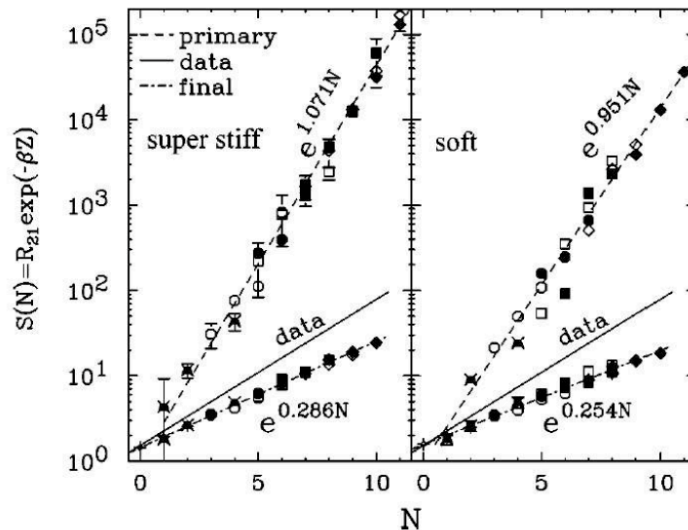


Fig. 8. Isoscaling plots calculated with SMF simulations before and after secondary decays for super stiff (left panel) and soft (right panel) density dependences of the symmetry energy.

significantly. The dynamical models relate the symmetry energy in the above equation to that of the fragmenting source. The statistical models, on the other hand, relate E_{sym} to that of the fragments formed at freeze-out. These conceptual differences between the statistical and the dynamical models are due to the radically different approaches taken in the interpretation of the multifragmentation process. In this respect one can say that the link between isoscaling parameters and symmetry energy depends on the way fragments are formed, while the observation of isoscaling and the relation to the $(Z/A)_{liq}$ value of the liquid phase appear as quite general properties and do not require the assumption of statistical equilibrium. Even the results on the symmetry energy extracted from fits to the isoscaling plots have conflicting interpretations when directly using Eq. (8). Conflicts arise from the different sequential decay effects predicted for the primary fragments by each model. As we already mentioned in the description of Fig. 4 (top panel), the isotopic distributions of fragments at the freeze-out stage, i.e. at the time they stop any nuclear interaction with one another and migrate towards the detectors solely under the effect of the Coulomb interaction, differ from the one that arises directly at the time of multifragmentation. This difference is due to secondary decays by excited primary fragments. These primary “hot fragments” are excited and cool down by decaying into light particle emission, thus changing their (Z,A) content. The final isotopic distributions of secondary “cold fragments” are different than those of the primary “hot fragments”. The isoscaling parameter α , in Eq. (8) corresponds to the hot

primary fragments which undergo sequential decay into cold secondary fragments. These secondary fragments are the ones that are eventually detected in experiments. The experimentally determined isoscaling parameter must therefore be corrected for the sequential decay effect before comparing it to theoretical models. The conflicting interpretations are evident when one observes that statistical model calculations show no significant change in the isoscaling parameter after sequential decay [44], dynamical models give contrasting results; with some showing no significant changes [45], while others showing a change of as much as 50% [46]. As an example we show on Fig. 8 the isoscaling function $S(N)$ obtained with SMF simulations of $^{112,124}\text{Sn}+^{112,124}\text{Sn}$ at $E/A=50$ MeV and when considering hot primary fragments (dashed line) and cold fragments after secondary decays (dot dashed line) [47]. The data points on the left (right) panel are obtained when one inputs a stiff (soft) density dependence of the symmetry energy in the simulation (see Fig. 5) [47]. The solid line corresponds to the experimental data of Ref. [33]. The primary fragments are characterized by an isoscaling slope $\alpha=1.07$ (left panel) and 0.95 (right panel) when using a stiff or soft symmetry energies, respectively. Any comparison to experimental data need to be performed using fragments distributions obtained after secondary decays. Fig. 8 clearly show that, besides the impossibility of reproducing the experimentally measured isoscaling slope, secondary decays strongly modify the value of α . As a consequence, any quantitative information on the symmetry energy and its density dependence (whether a soft or a stiff functional is more suited to the experimental measurements) strongly depends on the implementation of the late secondary decay stage in the calculations. The investigation results to be model-dependent. On the other hand statistical models lead to a different conclusion leaving hopes to use isoscaling and isospin distillation to probe the symmetry energy [44]. In Ref. [39] the authors have studied several reaction systems with different N/Z asymmetries ($^{40}\text{Ar}, ^{40}\text{Ca}+^{58}\text{Fe}, ^{58}\text{Ni}$ at $E/A=25, 45, 53$ MeV and $^{58}\text{Fe}, ^{58}\text{Ni}+^{58}\text{Fe}, ^{58}\text{Ni}$ at $E/A=30, 40$ and 47 MeV). They have used both statistical and dynamical models to study isoscaling distributions as a function on the incident energy. Assuming a density dependence of the symmetry energy as in Eq. (4), a value of $C_{\text{sym}}=31.6$ MeV and $\gamma=0.69$ were obtained (see dashed line on Fig. 9), thus excluding “very stiff” dependences as those reported with dotted and dot-dashed lines on Fig. 9. Using an Antisymmetrized Molecular Dynamics model

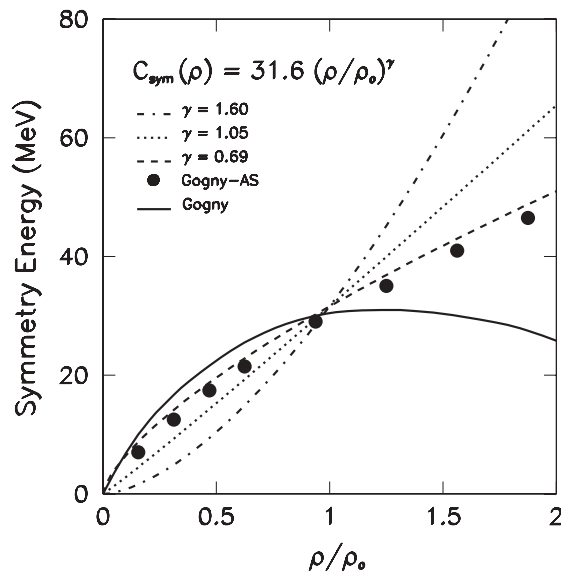


Fig. 9. Results on the density dependence of the symmetry energy obtained in Ref. [39].

(AMD) with explicit nuclear interactions in [41,46], the obtained results seem to support Gogny-AS forces, thus excluding also “very soft” density dependences as those that would correspond to a Gogny nuclear interaction (solid line on Fig. 9). Even if these conclusions about the symmetry energy and its density dependence may remain model dependent and possibly affected by secondary decay distortions, they represent one of the most interesting results in the field of isotopic effects in nuclear dynamics.

Other very important results from isoscaling probes of the symmetry energy have been reported by the INDRA-ALADIN collaboration [42], by studies of Dubna data on target fragmentation induced by energetic light projectiles [40] and by another work at Texas A&M University where access to

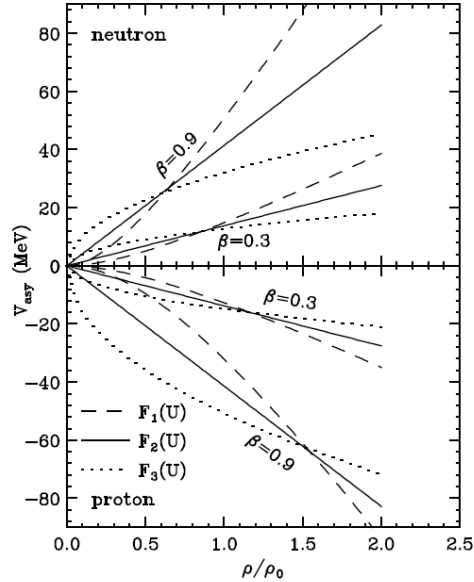


Fig. 10. Density dependence of the symmetry potential for neutrons (top panel) and for

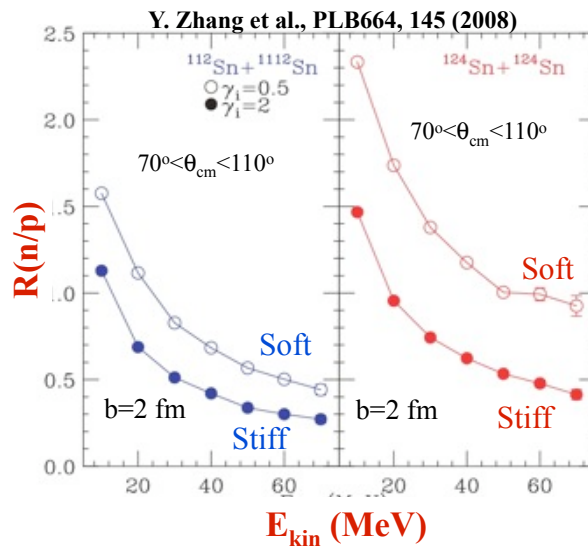


Fig. 11. Effects of the density dependence of the symmetry energy on the ratio between neutron and proton yields as a function of the kinetic energy in the center of mass. Taken from Ref. [50]

the very low density dependence of the symmetry energy has been achieved for the first time [48].

III.B Pre-equilibrium proton and neutron emissions

As already mentioned at the beginning of Section III heavy-ion collisions are characterized by pre-equilibrium phenomena consisting of a fast emission of light particles, especially free nucleons. The relative yields on protons and neutrons have been suggested to represent one of the strongest probes of the symmetry energy [49]. In order to understand this strong relation between pre-equilibrium emissions and the symmetry energy it is instructive to consider the symmetry potential

in nuclear matter. The potential acting on neutrons is indicated as $V_{Asy}^n(\rho, \delta)$ while the potential acting on protons is indicated as $V_{Asy}^p(\rho, \beta)$. The symmetry potential depends on the density ρ and on the isospin asymmetry $\beta=(\rho_n-\rho_p)/(\rho_n+\rho_p)$ [5,49]. The symmetry potential is attractive for protons and repulsive for neutrons and Fig. 10 shows three parameterizations often used in dynamical model simulations of heavy-ion collisions, indicated as F_1 , F_2 and F_3 . The top and bottom panels refer to $V_{Asy}^n(\rho, \delta)$ and $V_{Asy}^p(\rho, \delta)$, respectively. F_1 is the stiffest density dependence and F_3 is the softest one. Due to these different signs of the potential acting separately on neutrons and protons their kinetic energies can be strongly affected by different density dependences. For protons, the nuclear mean-field potential also includes a Coulomb term V_{Coul}^p . The competition between the Coulomb and the symmetry potential then leads to possible differences in the yields and energy spectra of protons and neutrons as well as on other isospin effects. Because of the relatively small values of $V_{Asy}^{n,p}(\rho, \beta)$, one needs to select observables that are sensitive to the asymmetric part but not the symmetric part of the nuclear EOS/potential in extracting information about the symmetry energy/potential from the experimental data [5].

The neutron/proton ratio of pre-equilibrium nucleons is among first observables that were proposed as possible sensitive probes of the symmetry energy [49]. The symmetry potential has following effects on preequilibrium nucleons. First, it tends to make more neutrons than protons unbound. One therefore expects that a stronger symmetry potential leads to a larger ratio of free neutrons to protons. Second, if both neutrons and protons are already free, the symmetry potential makes neutrons more energetic than protons. As an example, central collisions of $^{112}\text{Sn}+^{112}\text{Sn}$, $^{124}\text{Sn}+^{124}\text{Sn}$ and at a beam energy of 50 MeV/nucleon were studied using the ImQMD transport model in Ref. [50]. Fig. 11 shows the ratio between protons and neutrons emitted around 90° in the center of mass of the reaction, $R(n/p)$, as a function of their kinetic energies. It is observed that the magnitude of the $R(n/p)$ ratio strongly depends on whether the density dependence of the symmetry energy is stiff or soft. The effects of the symmetry energy increase with the neutron-asymmetry of the reaction system, being larger in the $^{124}\text{Sn}+^{124}\text{Sn}$ reaction (right panel) than in the $^{112}\text{Sn}+^{112}\text{Sn}$ reaction (left panel). The different stiffness of the symmetry in the model is modulated with the γ_i having the same meaning as γ in Eq. (4). Fig. 11 already shows that the n/p ratios are sensitive to the symmetry energy. However residual, non-symmetry energy effects may still exist due to the fact that protons are affected by the repulsion imposed by the Coulomb field and by secondary decay emission that can modify the yields on n and p especially at low kinetic energies. It has therefore been suggested to use the so-called “double n/p ratios”, $DR(n/p)$, defined as

$$DR(n/p) = \frac{R_{^{124}\text{Sn}+^{124}\text{Sn}}(n/p)}{R_{^{112}\text{Sn}+^{112}\text{Sn}}(n/p)} \quad (9)$$

with the numerator evaluated in the neutron-rich reaction system and the denominator evaluated in the neutron-poor reaction system. This double ratio is expected to remove most of the residual effects that do not depend on the symmetry energy. Indeed these residual effects act the same way in each of the two studied reactions and are therefore cancelled out in the double ratio.

These ideas have stimulated the proposal of an experiment at Michigan State University [51] that has resulted in very successful conclusions about the density dependence of the symmetry energy. This experiment (described in details in Ref. [51]) has used neutron wall detectors, made of liquid scintillators, to detect neutrons emitted in Sn+Sn reactions. Protons were detected by the LASSA array of Ref. [31]. Fig. 12 shows the obtained experimental results. The stars in the left panel of show the resulting neutron proton double ratios measured at $70^\circ \leq \theta_{CM} \leq 110^\circ$ as a function of the center-of-mass (CM) energy for nucleons emitted in central collisions [52]. Calculations have been performed for the studied reaction systems using the ImQMD model of Ref. [50]. The lines in the left panel of Fig. 12 show the calculated double ratios. Despite the large experimental uncertainties for higher energy data, these comparisons rule out both very soft ($\gamma_i=0.35$, dotted line with closed diamond points) and very stiff ($\gamma_i=2.0$, dotted line with open diamond symbols) density-dependent symmetry terms. The right panel shows the γ_i -dependence of the total χ^2 computed from the difference between predicted and measured double ratios. The performed χ^2 analysis has

suggested a value for the γ -parameter of about $\gamma=0.7\pm 0.3$, ruling out very stiff and very soft density

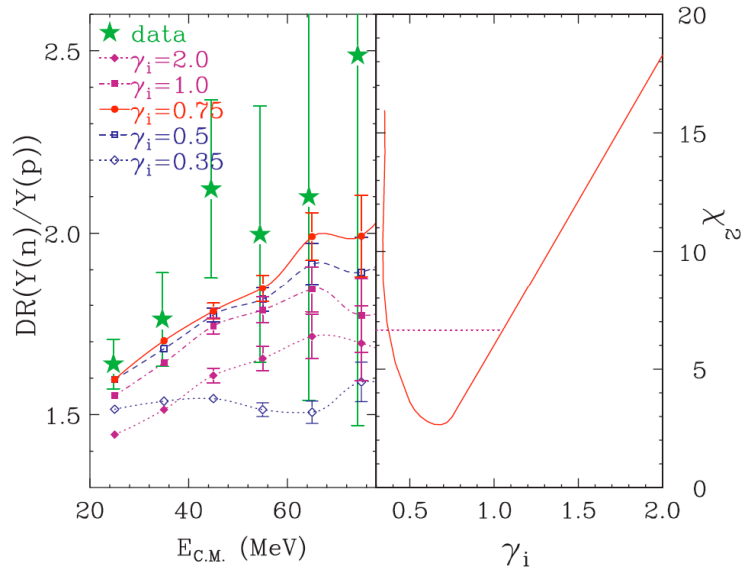


Fig. 12. Left panel: Neutron/proton double ratios as a function of their kinetic energies in the center of mass. Right panel: χ^2 analysis of neutron/proton double ratios as a function of the stiffness of the density dependence of the symmetry energy

dependences. This result on pre-equilibrium emissions is not affected by the problems encountered with fragment isotopic yields in Section III.A when studying isoscaling probes of the symmetry energy. However, it is remarkable that the value of γ obtained from Fig. 12 [52] are in good agreement with the analysis performed in Ref. [39], thus suggesting that even isoscaling analysis results have provided insightful information about the density dependence of the symmetry energy.

IV – STUDIES OF PERIPHERAL AND MID-PERIPHERAL COLLISIONS

Fig. 4 (bottom and middle panels) shows the schematic features of a collision at non-central impact parameters, $b_{red}=b/b_{max}>0.4$. These collisions mostly display a binary character with the formation of quasi-projectile and quasi-target partners that exchange particles thus changing their N/Z identity and getting excited. The density dependence of the symmetry energy has important effects on “isospin transport” consisting of the “diffusion and drift” of neutrons and protons during the collision between two heavy-ions in close contact [53,54]. In particular isospin diffusion has recently become one of the most sensitive observables to probe the density dependence of the symmetry energy in heavy-ion collisions [55,56,52]. Furthermore isospin diffusion can be used to study the degree of equilibration achieved during heavy-ion collisions providing probes for the expected hierarchical time evolution of different degrees of freedom [57].

IV.A Isospin transport: diffusion and drift

As already mentioned in Section II in peripheral collisions it is possible to identify projectile-like (PLF or QP) and target-like (TLF or QT) residues in model calculations, as well as in experiments. Calculations suggest that at incident energy above 30MeV per nucleon and for charge-asymmetric reactions, the symmetry term of the nuclear EOS provides a significant driving force that speeds up the isospin equilibration between the two reaction partners. Thus peripheral collisions may allow one to measure the time scales for charge and mass transport and diffusion. The degree of equilibration, correlated to the interaction time, should provide some insights into transport properties of fermionic systems and, in particular, give information on transport coefficients of asymmetric nuclear matter [54].

What do we mean by “diffusion and drift” processes in isospin transport? Both refer to an exchange of nucleons between the interacting projectile and target through their contact window

(see middle and bottom panels on Fig. 4). However the conditions that induce diffusion and drift are different. Isospin diffusion is caused by an isospin gradient between projectile and target: in other terms, it occurs when $(N/Z)_{proj} \neq (N/Z)_{targ}$ and neutrons and protons are exchanged so as to equilibrate the overall $(N/Z)_{total}$ of the system. Isospin drift occurs even in absence of isospin gradients. It is caused by the existence of density gradients into the system: in the presence of regions of nuclear matter at low density in contact with other high density portions, a migration of nucleons occurs so as to increase the neutron content of the low density regions leaving the higher density regions more N/Z-symmetric.

These migration processes typically occur in mid-peripheral reactions (see Fig. 4) where a low density “neck” region is formed between the interacting QT and QP that mostly remain at the original saturation density.

In N/Z asymmetric systems, isospin transport can arise from isospin gradients (diffusion) and from density gradients (drift). Through the low-density neck region, density gradients may be present also in binary systems. The neutron-excess is pushed towards the low-density region because this situation is energetically more favorable. This mechanism can induce isospin transport even in reactions between nuclei with the same $N=Z$ [58].

The role of the EOS in isospin transport mechanisms can be made more explicit by studying the response of nuclear matter, in the presence of neutron and proton density gradients. Since we are mostly facing situations where local thermal equilibrium is reached, we will discuss results obtained within the hydrodynamic limit, where the derivation of the isospin transport coefficients is more transparent. In such a framework the proton and neutron migration is dictated by the spatial gradients of the corresponding chemical potentials [43,54].

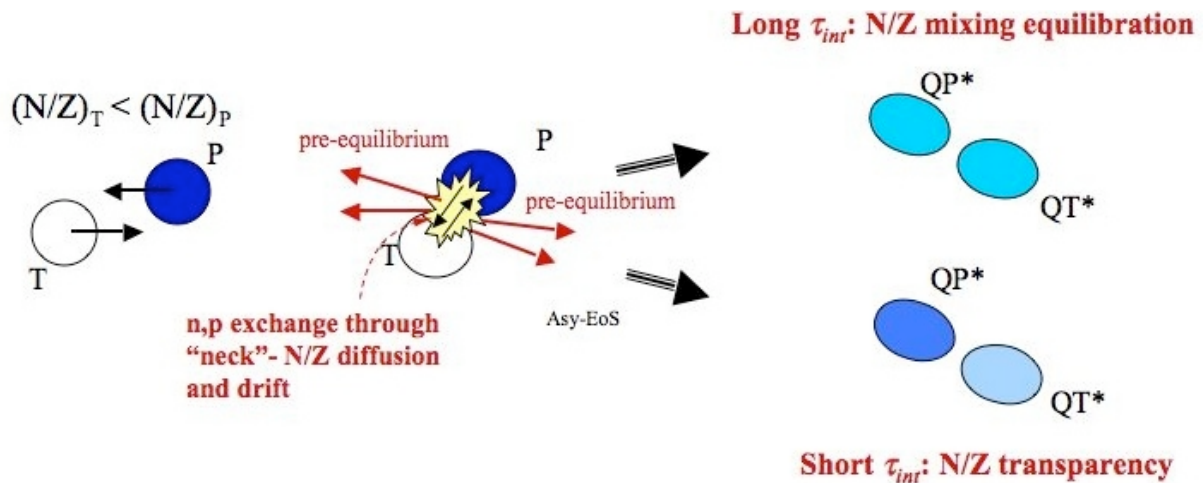


Fig. 13. Schematic drawing of the dynamical evolution of a mid-peripheral collision where isospin diffusion and drift occur.

Fig. 13 shows a schematic view of the dynamical evolution of the N/Z asymmetry of projectile (P) and target (T) nuclei during a mid-peripheral reaction where both isospin diffusion and isospin drift occurs. The original P and T have different N/Z-asymmetries as it is indicated by the different colors. During their interaction they exchange neutrons and protons (n and p) through the neck region: both diffusion and drift occur as a consequence of existing isospin and density gradients, respectively. This nucleon exchange occurs during the interaction between P and T and does not last forever. Indeed, depending on the incident energy and on the impact parameter, the two reaction partners stay in contact for a certain amount of time τ_{int} , after which they separate and migrate towards the detectors. If the interaction time is long enough, then the final QP and QT will possibly be characterized by the same N/Z-asymmetry (upper right side of Fig. 13, with QP and QT represented by the same color). This is the condition of complete “N/Z mixing” or “N/Z equilibration”: the N/Z asymmetry is uniformly distributed overall the dinuclear system. Whereas, if the interaction time, τ_{int} , is not long enough to achieve complete equilibration, then the final QP and QT will have isospin asymmetries that have not completely mixed and still keep memory of the initial isospin asymmetries of the original Q and T (lower right side of Fig. 13). This is the condition of “N/Z translucency” or “N/Z partial transparency”. The extent to which the system achieve a

condition of isospin equilibration or translucency depends on the symmetry energy and on the interaction time.

What is the connection between isospin transport and the symmetry energy? Isospin diffusion (transport in the presence of isospin gradients) bears information about the value of the symmetry energy at low density, while the drift (transport in the presence of density gradients) is more connected to the derivative of the symmetry energy. Therefore a detailed study of N/Z sharing between the quasi-projectile (QP*) and quasi target (QT*) provides a strong probe of the density dependence of the symmetry energy [52,55,59,60].

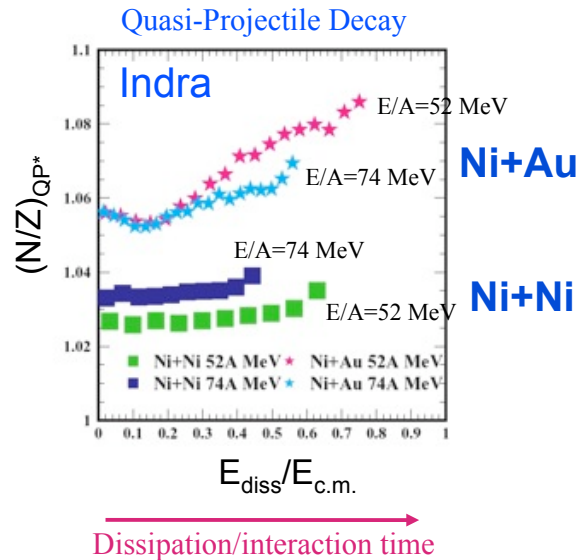


Fig. 14. N/Z asymmetry of the QP produced in Ni+Ni and Ni+Au collisions at E/A=52 and 74 MeV as a function of the dissipated energy. See text for details.

IV.B Experimental probes of isospin diffusion

The best way to study isospin diffusion consists of a complete reconstruction of the QP* and QT* sources schematically drawn on Fig. 13. This is not easy because the QT and QP are excited and decay by emitting particles and eventually breaking-up into fragments. Therefore the occurrence of isospin diffusion can be probed only by detecting the products of the decay of these two reaction partners and try to reconstruct their initial properties. In this lecture we will show two typical experiments that have been conducted at GANIL and MSU in the last couple of years. The GANIL experiment was performed with the Indra multidetector array [18] and consisted of studying the collisions $^{58}\text{Ni}+^{58}\text{Ni}$ and $^{58}\text{Ni}+^{197}\text{Au}$ at E/A=53 and 74 MeV [59]. In these two reaction systems the projectile is always ^{58}Ni with an asymmetry $(N/Z)_{\text{proj}} \sim 1.07$. The authors of Ref. [59] compared the results obtained in a N/Z-symmetric reaction, $^{58}\text{Ni}+^{58}\text{Ni}$ with $(N/Z)_{\text{proj}} = (N/Z)_{\text{targ}} \sim 1.07$ with those obtained when using a very neutron-rich target as ^{197}Au with $(N/Z)_{\text{targ}} \sim 1.5$. According to what we have explained in the previous subsection IV.A one expects to have a strong isospin diffusion process in the $^{58}\text{Ni}+^{197}\text{Au}$ reaction because of the large N/Z difference between projectile and target. In the case of the other symmetric reaction, $^{58}\text{Ni}+^{58}\text{Ni}$, one expects to have reduced nucleon migration processes only due to isospin drift and not to isospin diffusion. Fig. 13 schematically shows the importance of the reaction time between projectile and target, depending on the impact parameter and the incident energy. In order to observe a significant isospin diffusion process in the N/Z-asymmetric reaction $^{58}\text{Ni}+^{197}\text{Au}$ the interaction time has to be large enough. Therefore one expects larger isospin diffusion phenomena at lower incident energies, E/A=52 MeV, rather than at higher energies, E/A=74, and at smaller impact parameter. In Ref. [59] the “dissipated energy” observable has been used to provide an estimate of the interaction time, E_{diss} . In order to construct the dissipated energy the authors of Ref. [59] have collected event by event all the fragments produced by the decay of the QP*. If no energy was dissipated between projectile and target, the whole kinetic energy initially available for reaction, E_{CM} , would be entirely converted into the kinetic

energy of the QP* and QT*, $E_{CM} = 1/2 \cdot \mu \cdot v_{rel}^2$, with μ and v_{rel} being, respectively, the reduced mass and the relative velocity between QT* and QP*. Whereas, QT and QP can be excited at the expenses of the kinetic energy in the center of mass, E_{CM} . Then the kinetic energy of the relative motion of the QP and QT will be smaller than E_{CM} , and the difference is therefore the “dissipated energy”, $E_{diss} = E_{CM} - 1/2 \cdot \mu \cdot v_{rel}^2$. The construction of the E_{diss} observable requires the detection and identification of all fragments produced in the decay of the quasi-projectile QP* with the Indra detector array [18]. Once reconstructed E_{diss} provides an indirect estimate of the interaction time between projectile and target. Long interaction times correspond to strong dissipation (high E_{diss}). Short interaction times correspond to small dissipations (low E_{diss}). With all the fragments produced by the decay of the QP* its N/Z asymmetry was also measured, $(N/Z)_{QP^*}$. Fig 14 represents the measured correlation between $(N/Z)_{QP^*}$ and E_{diss}/E_{CM} for Ni+Au and Ni+Ni collisions at different incident energies (see labels close to data points). It is observed that, regardless the incident energy, the N/Z of the QP remains almost unmodified with increasing dissipation in the case of N/Z-symmetric reactions, Ni+Ni, where no significant isospin diffusion phenomena are expected to occur. The situation is quite different in the case of Ni+Au collisions. As the dissipation (and therefore the interaction time) increases, the N/Z of the QP, originated by the Ni projectile nucleus ancestor, increases significantly. This increase is caused by isospin diffusion from the neutron-rich Au target. At lower incident energies, $E/A=52$ MeV, the interaction time and dissipation can be larger and therefore the N/Z of the QP* can increase more as compared to the quicker reaction at $E/A=74$ MeV. This results is an experimental indication of isospin diffusion phenomena in heavy-ion collisions. The same data of Ref. [59] were then used to probe the density dependence of the symmetry energy using an SMF dynamical model [60]. The correlation between $(N/Z)_{QP^*}$ and E_{diss}/E_{CM} was calculated and compared to experimental data. The comparison has provided an indication of a stiffness of the symmetry energy corresponding to Eq. (4) with a value of unity for the parameter γ , i.e. $\gamma \sim 1$ not far from the values obtained with pre-equilibrium n/p emissions and isoscaling probes (see previous sections).

In another experiment performed at MSU [55] with the LASSA array [31], isospin diffusion was studied in peripheral $^{112}\text{Sn}+^{112}\text{Sn}$, $^{112}\text{Sn}+^{124}\text{Sn}$, $^{124}\text{Sn}+^{112}\text{Sn}$ and $^{124}\text{Sn}+^{124}\text{Sn}$ collisions at $E/A=50$ MeV. In particular in the study of collisions between nuclei with different isospin asymmetries such as $^{112}\text{Sn}+^{124}\text{Sn}$ one expects a strong diffusion of nucleons from the neutron-rich system, ^{124}Sn , to the more symmetric ^{112}Sn reaction partner. In Ref. [55] this isospin diffusion between ^{112}Sn target and ^{124}Sn projectile nuclei has been studied by means of the so-called “imbalance ratios”

$$R_i = \frac{2X_i - X_{A+A} - X_{B+B}}{X_{A+A} - X_{B+B}} \quad (10)$$

where X is an isospin sensitive observable which is a linear function of the asymmetry, $\delta=(\rho_n-\rho_p)/(\rho_n+\rho_p)$, of the emitting source. For the two symmetric systems $^{124}\text{Sn}+^{124}\text{Sn}$ and $^{112}\text{Sn}+^{112}\text{Sn}$, R_i is automatically normalized to +1 and -1, respectively. Experimentally one does not have direct access to the δ -asymmetry of the emitting sources. In the experiment described in Refs. [55,56] the X-observable was constructed by using the slope of the isoscaling analysis of measured isotopic distributions or the $^7\text{Li}/^7\text{Be}$ isobaric yield ratios. In the limit of isospin equilibrium, $R_i=0$. On the left panel of Fig. 15 the R_i ratios extracted from the $^7\text{Li}/^7\text{Be}$ yield ratios are represented as a function of the rapidity, $y=1/2 \cdot [\log(1+\beta_{//})]/[\log(1-\beta_{//})]$, of the detected fragments, normalized to the rapidity of the beam, $y/y_{beam} \sim 1$. Whereas fragments emitted by the QP* decay move with a rapidity close to the target, $y/y_{beam} \sim 0$.

It is observed that around projectile (target) rapidity the “imbalance ratio” is equal to about 0.5 (-0.5). If complete isospin mixing and equilibration occurred, one would have expected to observe $R_i=0$ at both projectile and target rapidities, as a consequence of a uniform N/Z distribution along the dinuclear system. On the other hand, in case of isospin transparency, one would have observed $R_i=+1$ (-1) at projectile (target) rapidity. The observation of $R_i \sim 0.5$ implies that the N/Z is not completely equilibrated in the collision and therefore the occurrence of “isospin translucency”: the interaction time is not long enough to achieve equilibration. This observed phenomenon is used to probe the density dependence of the symmetry energy [52]. The right panel of Fig. 15 shows the positive rapidity side of the left panel (data points) and the lines refer to calculations

performed with the ImQMD model [50,52] by using different parameterizations of the symmetry energy with different values of the γ_i parameter in the range $0.35 \leq \gamma_i \leq 2.0$ [52]. Using the χ^2 criterion

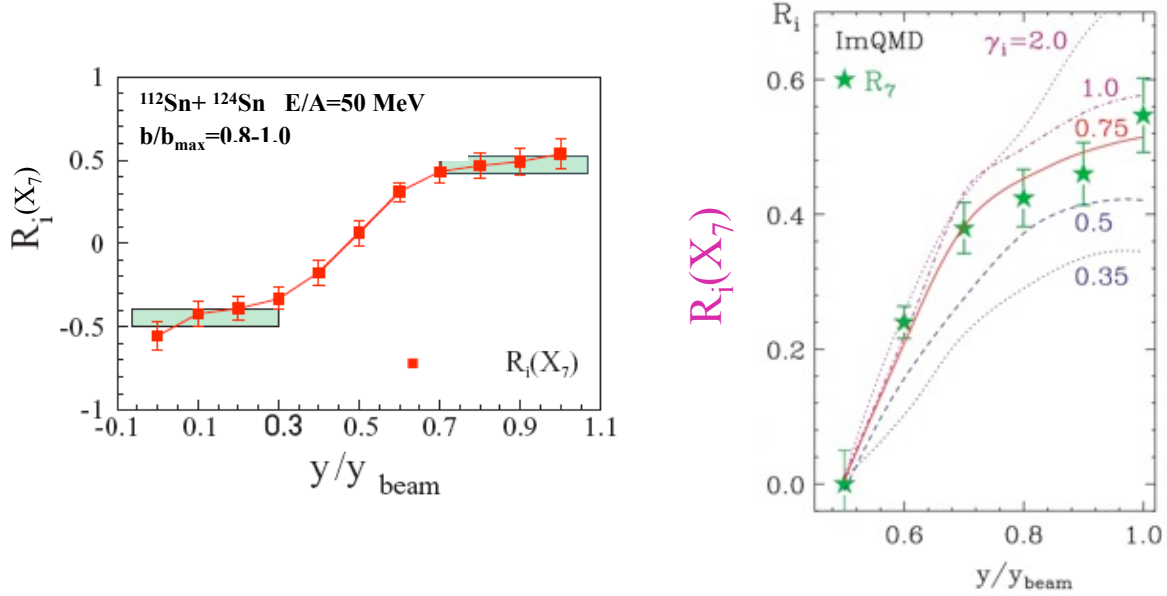


Fig. 15. Rapidity dependence of the imbalance ratio constructed with $^7\text{Li}/^7\text{Be}$ isobaric ratios in $^{112}\text{Sn} + ^{124}\text{Sn}$ collisions at $E/A = 50$ MeV. The lines on the right panel correspond to calculations with the ImQMD model.

adopted previously in Fig. 12, the analysis favors the region $0.45 \leq \gamma_i \leq 0.95$. Similar analyses on the same data and using different isospin sensitive X observables (see Eq. (10)) favor the region $0.44 \leq \gamma_i \leq 1.0$, see Ref. [52].

V – PRESENT STATUS AND FUTURE PERSPECTIVES

The results obtained with isospin diffusion (this section) and n/p pre-equilibrium emissions (Sections III.B and IV.B) show that a consistent picture exists to describe the density dependence of the symmetry energy using the same model calculations, i.e. ImQMD. This results has been presented as one of the most firm constraints on the symmetry energy at sub-saturation density. In this respect one can conclude that all the experimental probes provided so far have suggested a density dependence of the symmetry energy with a functional form as in Eq. (4) and with an exponent in the range $0.4 < \gamma < 1$ which excludes both very stiff and very soft symmetry energies. It must be stressed out that even isoscaling probes provide results consistent with this range regardless of their possible uncertainties due to secondary decay effects [39].

As already mentioned in Section II when discussing Eqs. (2) and (3), the results obtained from heavy-ion collision experiments can be described in terms of the value of the symmetry energy at saturation density, $S_0 = E_{\text{sym}}(\rho_0)$, and the L and K_{sym} parameters, i.e. the first and second derivative at saturation. These values define the density dependence of the symmetry energy and provide a link to other fields on nuclear physics and astrophysics. For realistic parameterization of $E_{\text{sym}}(\rho)$, K_{sym} is strongly correlated to L [61]. As the second term in Eq. (4) is much larger than the third term, we believe L can be determined more reliably than K_{sym} . Furthermore, the slope parameter, L is related to p_0 , i.e. the pressure from the symmetry energy for pure-neutron matter at saturation density. The symmetry pressure, p_0 , provides the dominant baryonic contribution to the pressure in neutron stars at saturation density [5,62–64].

The authors of Ref. [52] have performed a detailed χ^2 analysis to locate the approximate boundaries in the S_0 and L plane that well reproduces isospin diffusion data. The two diagonal lines in Fig. 16, taken from Ref. [52] represents estimates in such an effort. The dashed, dot-dashed, and solid lines centered around $S_0 = 30.1$ MeV in Fig. 16 represents L values consistent

with the analysis presented in Figs. 12 and 15 [52]. The vertical line at $S_0=31.6$ MeV depicts the range of L values obtained from comparisons of IBUU04 [5] calculations to the measured isospin

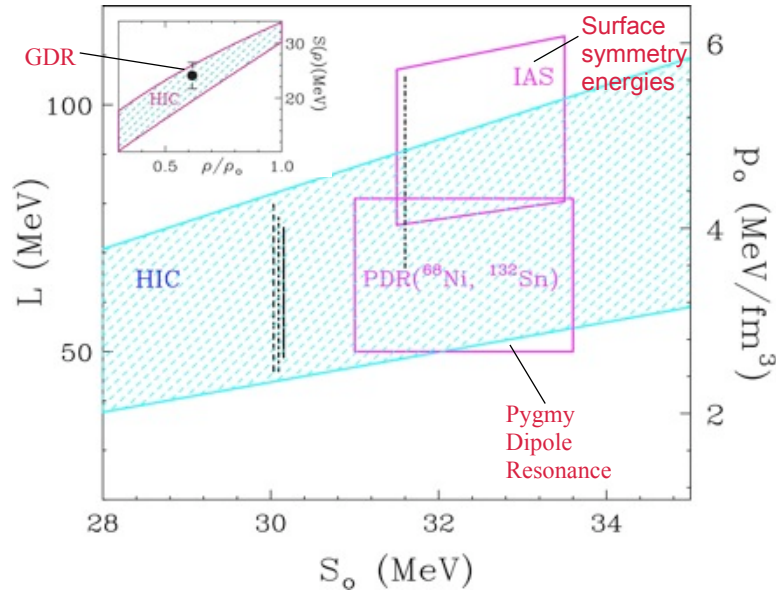


Fig. 16. Constrains in the S_0 , L and ρ_0 parameters of Eq. (2) and (3) from heavy-ion collision data, pygmy and giant dipole resonance research and from systematics of surface symmetry energies.

diffusion data in the left panel of Ref. [55]. Constraints from the isoscaling analyses discussed in Section III.A are not included even if they are in good agreement with these conclusions. Fig. 16 also reports, other recent constraints in the density dependence of the symmetry energy. The lower box centered at $S_0=32$ MeV depicts the range of ρ_0 values from analyses of pygmy dipole resonance (PDR) data [66]. The values of ρ_0 are given in the right axis. The upper box centered at $S_0=32.5$ MeV depicts the constraints reported in Ref. [61] from the analyses of nuclear surface symmetry energies. The shaded region in the inset of Fig. 17 shows the density dependence of the symmetry energy of the shaded region bounded by $S_0=30.2$ and 33.8 MeV, the limiting S_0 values given by the PDR data [66]. The range S_0 adopted here is consistent with the finding from the charge exchange spin-dipole resonance result [67]. The giant dipole resonances (GDR) result of Refs. [68,69] is plotted as a solid circle in the inset.

Fig. 16 can be considered as a summary of the present status on the density dependence of the symmetry energy below saturation density, $\rho < \rho_0$. Significant efforts will be important in the future in order to improve the existing constrains. Indeed, especially in the field of neutron star properties the present error bars do not allow to draw unambiguous conclusions. The future availability of radioactive beam facilities will allow to set better constrains. Indeed, collisions with larger isospin asymmetries, N/Z , will be studied. The effects of the symmetry energy will be enhanced and the sensitivity of different observables will be better explored improving the analysis and the comparisons to theoretical calculations.

Regardless the success obtained so far, the density dependence of the symmetry energy remains still largely unconstrained at supra-saturation densities, $\rho > \rho_0$. Significant experimental efforts will be required in that field with heavy-ion collisions at energies about 200 MeV/nucleon. Similar experiments will be performed at the Fair facility in Germany, Riken in Japan and FRIB in the USA. At these high energies nuclear matter is compressed up to $2-3\rho_0$ where probes of the symmetry energy will include squeeze-out neutron/proton emissions and collective flow and meson production (π^-/π^+ and K^0/K^+ yield ratios). Very exciting perspectives exist, involving new technologies and new physics insights towards a better understanding of the equation of state of asymmetric nuclear matter.

BIBLIOGRAPHY.

- [1] J. Xu, L.W. Chen, B.A. Li, H.R. Ma, Phys. Rev. C 77 (2008) 014302.
- [2] Isospin Physics in Heavy-Ion Collisions at Intermediate Energies, Eds. Bao-An Li and W. Udo Schroeder (Nova Science Publishers, Inc, New York, 2001).
- [3] A.E.L. Dieperink, Y. Dewulf, D. Van Neck, M. Waroquier, V. Rodin, Phys. Rev. C 68 (2003) 064307.
- [4] J.M. Lattimer, M. Prakash, Science 304 (2004) 536.
- [5] Bao-An Li, Lie-Wen Chen, Che-Ming Ko, Phys. Rep. 464, 113 (2008)
- [6] Introductory Nuclear Physics, K.S. Krane, Ed. Wiley (1987)
- [7] A.E.L. Dieperink, Y. Dewulf, D. Van Neck, M. Waroquier, V. Rodin, Phys. Rev. C 68 (2003) 064307
- [8] A.W. Steiner, .A. Li, Phys. Rev. C 72 (2005) 041601 (R).
- [9] B.A. Brown, Phys. Rev. Lett. 85 (2000) 5296.
- [10] C.J. Horowitz, J. Piekarewicz, Phys. Rev. Lett 86 (2001) 5647; Phys. Rev. C 64 (2001) 062802 (R); Phys. Rev. C 66 (2002) 055803.
- [11] S. Typel, B.A. Brown, Phys. Rev. C 64 (2001) 027302.
- [12] M. M. Sharma, et al., Phys. Rev. C 38 (1988) 2562.
- [13] S. Shlomo, D. H. Youngblood, Phys. Rev. C 47 (1993) 529.
- [14] T. Li, et al., Phys. Rev. Lett. 99 (2007) 162503.
- [15] "Dynamics and Thermodynamics with Nucleonic Degrees of Freedom", Eur. Phys. J. A30, 121 (2006) and Refs. therein.
- [16] C. Cavata et al., Phys. Rev. C 42, 1760–1763 (1990).
- [17] L. Phair et al., Nucl. Phys. A 548, 489 (1992).
- [18] J. Pouthas et al., Nucl. Instr. and Meth. in Phys. Res. A357 (1995), 418.
- [19] A. Pagano et al, Nucl. Phys. A 734 (2004) 504.
- [20] J. Lecomte et al., Phys. Lett. B 391, 317 (1994).
- [21] E. Geraci et al., Nucl. Phys. A 734, 524 (2004).
- [22] J. Łukasik et al., Phys. Rev. C 55, 1906 (1997).
- [23] M. Di Toro et al., Eur. Phys. J. A 30 (2006) 253.
- [24] S. Piantelli et al., Phys. Rev. Lett. 88, 052701 (2002).
- [25] S. Hudan et al., Phys. Rev. C 71, 054604 (2005).
- [26] D. Theriault et al., Phys. Rev. C71, 014610 (2005).
- [27] E. De Filippo et al. , Phys. Rev. C71 (2005).
- [28] H. Muller, B. Serot, Phys. Rev. C 52 (1995) 2072.
- [29] M. Di Toro et al., arXiv:1003.2957v1 [nucl-th].
- [30] S. Das Gupta, A.Z. Mekjian, M.B. Tsang, Adv. Nucl. Phys. 26, 91 (2001).
- [31] B. Davin et al., Nucl. Instr. and Meth. A 456 (2001), p. 290
- [32] R.T. De Souza et al., Nucl. Instr. Meth. A 295, 109 (1990)
- [33] M.B. Tsang et al., et al., Phys. Rev. Lett. 86, 5023 (2001).
- [34] D.V. Shetty, S.J. Yennello, E. Martin et al., Phys. Rev. C68, 021602 (2003).
- [35] G.A. Souliotis, M. Veselsky, D.V. Shetty et al., Nucl. Phys. A746, 526c (2004).
- [36] M.N. Andronenko, L.N. Andronenko, W. Neubert, Prog. Theor. Phys. Suppl. 146, 538 (2002).
- [37] M. Veselsky, G.A. Souliotis, M. Jandel, Phys. Rev. C 69, 044607 (2004).
- [38] H.S. Xu, et al., Phys. Rev. Lett. 85 (2000).
- [39] D. Shetty et al. Phys. Rev. C76, 024606 (2007).
- [40] A.S. Botvina et al., Phys. Rev. C65, 044619 (2002).
- [41] A. Ono, Phys. Rev. C68, 051601(R) (2003).
- [42] A. Le Fevre et al., PRL94, 162701 (2005).
- [43] M. Colonna and M.B. Tsang, Eur. Phys. J. A 30, 165, 182 (2006).
- [44] M. B. Tsang et al., Phys. Rev. C 64, 054615 (2001).
- [45] W. D. Tian et al., arXiv:nucl-th/0601079 (2006).
- [46] A. Ono et al., Phys. Rev. C 70, 041604(R) (2004).
- [47] T.X. Liu, M.J. van Goethem, X.D. Liu et al., Phys. Rev. C 69, 014603 (2004).
- [48] S. Kowalski et al., Phys. Rev. C75, 014601 (2007).
- [49] B.A. Li, C.M. Ko, Z.Z. Ren, Phys. Rev. Lett. 78 (1997) 1644.
- [50] Y. Zhang et al., Phys. Lett. B664, 145 (2008).
- [51] M.A. Famiano, et al., Phys. Rev. Lett. 97 (2006) 052701.

- [52] M.B. Tsang et al., Phys. Rev. Lett. 102, 122701 (2009)
- [53] M. Di Toro et al., Journal of Physics G: Nuclear and Particle Physics 37, 083101 (2010)
- [54] L. Shi and P. Danielewicz, Physical Review C 68, 064604 (2003)
- [55] M.B. Tsang et al., Physical Review Letters 92, 062701 (2004)
- [56] T.X. Liu et al., Physical Review C 76, 034603 (2007)
- [57] W.U. Schroeder et al. in: D.A. Bromley (Ed.), Treatise on Heavy-ion Science, vol. 2, Plenum, New York, London, 1984, p. P113
- [58] R. Lioni, V. Baran, M. Colonna, M. Di Toro, Phys. Lett. B 625, 33 (2005).
- [59] E. Galichet et al., Physical Review C 79, 064614 (2009).
- [60] E. Galichet et al., Physical Review C 79, 064614 (2009).
- [61] P. Danielewicz et al., Nucl. Phys. A 818, 36 (2009).
- [62] C. J. Horowitz et al., Phys. Rev. Lett. 86, 5647 (2001).
- [63] J. Piekarewicz, Phys. Rev. C 69, 041301 (2004).
- [64] Satoshi Yoshida and Hiroyuki Sagawa, Phys. Rev. C 73, 044320 (2006).
- [65] B. A. Li and L.W. Chen, Phys. Rev. C 72, 064611 (2005).
- [66] A. Klimkiewicz et al., Phys. Rev. C 76, 051603 (2007).
- [67] H. Sagawa et al., Phys. Rev. C 76, 024301 (2007).
- [68] L. Trippa et al., Phys. Rev. C 77, 061304(R) (2008).
- [69] G. Colo, arXiv:0902.3739.